

# Structural Engineering



---

## Modeling the EPRI-Wisconsin Power and Light Broken Wire Tests

by Alan B. Peabody  
March 2003

Structural Engineering Series No. 2003-01

Department of Civil Engineering  
and Applied Mechanics

TA633

S76

no. 2003-01

2003

F11

**McGill University**

Montreal

**Modeling the EPRI-Wisconsin  
Power and Light Broken Wire Tests**

by

Alan B. Peabody

March 2003



Department of Civil Engineering and Applied Mechanics

McGill University

Structural Engineering Series No. 2003-01

© Alan B. Peabody, 2003 All Rights Reserved

TAG 33  
576  
No. 2003-01  
2003  
PSE

## Abstract

Peyrot et. al. (1978) reported on full-scale tests performed on a double circuit 138-kV line owned by Wisconsin Power and Light. The line was slated for replacement with a new 345-kV line, making it available for destructive tests. The tests included broken wire tests at three tensions of IBIS conductor, 397.5 kcmil ACSR 26/7. These three tests were modeled using the finite element dynamics software package ADINA.

The broken wire tests showed two distinct peaks in the tension in the suspension insulator string adjacent to the break. The first when the insulator string is pulled in line with the conductor and the second when the conductor is retensioned at the bottom of its fall. The finite element model accurately predicts the timing and magnitude of the first peak. The timing of the second peak is also accurately predicted but the magnitudes are greater than those recorded in the tests.

This report is a draft of Chapter 4 of a Ph.D. thesis reporting research into mitigating the dynamic loads caused by broken wires.

## Sommaire

Des essais dynamiques en pleine grandeur ont été réalisés en 1978 sur une ligne biterne à 138 kV de la Wisconsin Power and Light et les résultats ont été publiés en détail par Peyrot et al. (1978). Cette ligne devait être démantelée ce qui en a fait une bonne candidate pour des essais destructifs. Parmi les essais réalisés, l'étude se concentre sur trois scénarios de bris de conducteur IBIS, 397.5 kcmil ACSR 26/7 à différents niveaux de tension mécanique initiale. Un modèle d'analyse dynamique par éléments finis de ces trois essais a été créé à l'aide du logiciel commercial ADINA, pour fins de validation.

Les essais de bris de conducteur ont indiqué deux pointes de tension bien distinctes dans la chaîne de suspension adjacente au point de bris. La première pointe se produit lorsque la chaîne d'isolateurs balance pour s'aligner avec le conducteur alors que la deuxième se produit lorsque le conducteur atteint le point le plus bas de sa chute et amorce une remontée. Le modèle d'éléments finis reproduit précisément l'occurrence et la grandeur de la première pointe. L'occurrence de la deuxième pointe est aussi prédite avec précision alors que son intensité est surestimée par le modèle.

Ce rapport est une version préliminaire du Chapitre 4 de la thèse de doctorat de l'auteur, traitant d'une recherche sur la mitigation des charges dynamiques induites par les bris de câbles.

# Table of Contents

## Chapter 4 Modeling the EPRI-Wisconsin Power & Light Tests

4.1	Introduction.....	1
4.2	Description of Tests .....	1
4.2.1	Tower Natural Frequency .....	1
4.2.2	Broken Conductor Tests .....	2
4.2.3	Inconsistencies in the Test Data.....	3
4.3	Analysis of the Broken Conductor Test Data .....	3
4.4	Finite Element Modeling .....	4
4.4.1	Tower Model.....	4
4.5	Modeling the Conductor .....	12
4.5.1	Introduction.....	12
4.5.2	Natural Frequencies and Mode Shapes of Conductor.....	15
4.5.3	Conductor Damping.....	15
4.6	Modeling of the Insulator Assemblies .....	19
4.7	Time History Analysis Results .....	20
4.7.1	Variations in the Model Parameters.....	23
4.8	Conclusions.....	25
4.9	Recommendations for Future Tests .....	26
	References .....	28

## Figures

## Appendix A – Conductor Natural Frequencies and Mode Shapes

## Appendix B – ADINA Model Parameters for EPRI – Wisconsin Power & Light Tests

## List of Figures

- 4-1 EPRI Wisconsin Test Line Profile
- 4-2 Wisconsin Test Towers
- 4-3 Ibis Conductor
- 4-4 Insulator Tension at Tower T3, Tests III L 1, 2 & 3
- 4-5 Fourier Spectra, Wisconsin Tests III L 2 & 3
- 4-6 Fourier Spectra, Space Truss Tower Model
- 4-7 Linear 2 DOF Spring-Mass System
- 4-8 Wisconsin Tests, Reduced Tower Model
- 4-9 Comparison of Full and Reduced Tower Models
- 4-10 Fourier Spectra Tower Model Comparison
- 4-11 Conductor Model
- 4-12 Insulator & Hardware Assembly models
- 4-13 Insulator Tension at Tower T3, Test III L3 vs ADINA Model
- 4-14 Frequency Content, Test III L3 and ADINA Model
- 4-15 High Frequency Content of Test III L3 and ADINA Model
- 4-16 Insulator Tension at Tower T3, Test III L3, ADINA Model vs ADINA Model  
with 10 Hz Low Pass Notch Filter
- 4-17 Insulator Tension at Tower T3, Test III L3, Comparison of 10 Hz and 15 Hz Low  
Pass Notch Filters
- 4-18 Insulator Tension at Tower T3 Test III L1 vs Filtered ADINA Model
- 4-19 Insulator Tension at Tower T3, Test III L2 vs Filtered ADINA Model
- 4-20 Insulator Tension at Tower T3, Test III L3 vs Filtered ADINA Model

- 4-21 Insulator Tensions Tower T3, ADINA Models of Tests III L1 to 3
- 4-22 Test III L3, Effect of Changes in Insulator Length
- 4-23 Insulator Tension at Tower T3, Test vs ADINA Model with Vertical Damping

## List of Tables

4-1	EPRI-Wisconsin Power & Light Broken Conductor Tests.....	2
4-2	Conductor Properties .....	4
4-3	Reaction Comparison.....	5
4-4	Deflection Comparison .....	6
4-5	Wisconsin Test Tower Deflections and Stiffnesses.....	7
4-6	Wisconsin Test Tower Frequencies .....	7
4-7	Comparison of Frequency Analysis and Plucking Analysis.....	8
4-8	Equivalent Mass, Stiffness and Damping .....	11
4-9	Longitudinal Material Properties .....	13
4-10	Axial Damping Ratios.....	17
4-11	Peak Test Magnitudes .....	23

## **Chapter 4**

### **Modeling the EPRI-Wisconsin Power and Light Tests**

#### **4.1 Introduction**

Peyrot et. al. (1978) reported on full-scale tests performed on a double circuit 138-kV line owned by Wisconsin Power and Light. Robert Kluge of American Transmission Co. kindly lent the author a film made about the tests (EPRI 1978). The line was slated for replacement with a new 345-kV line, making it available for destructive tests. The line was built in 1931 using lattice steel towers with square bases. The line had two 7 No. 8 Copperweld shield wires. The left circuit was strung with a 397 kemil ACSR 26/7 conductor and the right circuit with a 471A Anaconda cable with 7 hard drawn copper wires over a 3 wire calsun bronze core. The test section had 7 towers as shown in Figure 4-1 (Peyrot et al. 1978, Fig. 3.1). All of the wires were anchored to the ground at the ends of the test section. The outline of the towers is shown in Figure 4-2.

#### **4.2 Description of Tests**

Tests were performed to determine the natural frequency of the towers, the effect of a broken suspension insulator and the effect of broken conductors. Only the tests of natural frequency and broken wires are of interest here.

##### **4.2.1 Tower Natural Frequency**

Two tests to determine the natural frequency of the tower were performed, one with all of the wires attached to the tower with their normal suspension hardware and one with the shield wires detached. The tower was excited by tensioning a cable attached to the top of tower to approximately 9.8 kN (1000 kgf) and suddenly releasing it.

The static deflection was measured as 2 to 3 cm. The movement of the tower top was measured using an accelerometer. The period of the first mode of the tower with the shield wires detached is reported to be 0.25 s (4 Hz) with a damping ratio of 4%. With the shield wires attached, the period was reported to be 0.24 s (4.2 Hz) with a damping ratio of 7%.

#### 4.2.2 Broken Conductor Tests

Twelve broken conductor tests were performed as shown in Table 4-1. The tests of most interest are the tests of the ACSR conductor. Today, copper conductor is rarely used in the construction of new transmission lines. The majority of the existing high voltage and extra high voltage transmission systems use all aluminum, aluminum alloy or ACSR conductor.

**Table 4-1  
EPRI-Wisconsin Power & Light  
Broken Conductor Tests**

Test No.	Conductor	Effective I-String Length (m)	Starting Tension (kN)	Residual Static Tension (kN)
IIIR1	Copper/Bronze	2.2	18.66	11.00
IIIR2	Copper/Bronze	2.2	19.10	11.01
IIIR3	Copper/Bronze	2.2	Broken Arm	
IIIL1	ACSR	2.2	12.43	6.96
IIIL2	ACSR	2.2	17.77	8.69
IIIL3	ACSR	2.2	21.32	9.33
VR1	Copper/Bronze	4.3	15.99	7.55
VR2	Copper/Bronze	4.3	18.21	7.95
VR3	Copper/Bronze	4.3	Broken Arm	
VL1	ACSR	4.3	14.22	5.11
VL2	ACSR	4.3	No Load Cell Data	
VL3	ACSR	3.7	23.55	7.24

### **4.2.3 Inconsistencies in the Test Data**

The test report and film of the tests (EPRI 1978; Peyrot et al. 1978) have inconsistencies in the length reported for the span between Towers T3 and T4 (the span next to the breaks) and the length of the insulator strings. The first span was assumed to be 297 m. The insulator string was assumed to be 2.08 m long.

### **4.3 Analysis of the Broken Conductor Test Data**

For comparison with the finite element model being developed for this research project, the data from three of the EPRI Wisconsin tests were analyzed. The tests were performed at the top, center and lower left crossarms with three different conductor tensions – tests IIIIL1, IIIIL2, and IIIIL3 (see Table 4-1). All of the tests were performed using a 397 kcmil ACSR 26/7 conductor. This conductor matches standard Ibis ACSR which consists of a 7 strand steel cable overlaid with 26 strands of aluminum wire in two layers, see Figure 4-3. Table 4-2 (next page) shows the conductor properties reported by Peyrot et. al. (1978) and published conductor properties for Ibis conductor (Alcoa 1974; Farr 1980).

The time histories for Tests IIIIL1, 2 and 3 shown in Figure 6-4 of the report were digitized, resampled to have a uniform time step and scaled in Newtons. Figure 4-4 shows the time histories. Test IIIIL 1 had a gap in the time history for the 2<sup>nd</sup> peak. The timing and magnitude of the 2<sup>nd</sup> peak was taken from Table 6-2 of the report. Fourier analyses of the two complete time histories are shown in Figure 4-5. Both have a definite peak at a frequency of 1.35 Hz with a period of 0.75 s. The time

history of test IIL1 shows a bifurcated first peak. This may be due to incipient buckling of the crossarm noted by Kluge (2002).

**Table 4-2  
Conductor Properties**

Description	Peyrot et. al.	Published Values	
Stranding	26 / 7	26 / 7	
Name	-	Ibis	Ibis
Steel Area	-	32.8 mm <sup>2</sup>	0.0508 in <sup>2</sup>
Aluminum Area	-	201.2 mm <sup>2</sup>	0.3119 in <sup>2</sup>
Total Area	234.0 mm <sup>2</sup>	234.0 mm <sup>2</sup>	0.3627 in <sup>2</sup>
Diameter	-	19.9 mm	0.783 in
Unit mass	0.814 kg/m	0.813 kg/m	0.5466 lbm/ft
Average Density	-	3476 kg/m <sup>3</sup>	217 lbm/ft <sup>3</sup>
Rated Tensile Strength	68.5 kN	72.5 kN	16.3 kips
Final Modulus of Elasticity	69.6 GPa	74.2 GPa	10,760 ksi
Sag-Tension Chart No.	-	1-782 (No. 8)	

## 4.4 Finite Element Modeling

### 4.4.1 Tower Model

The tower was modeled as a pin-connected truss using ADINA (ADINA 2001). A static analysis was performed for comparison with the tower deflections included in Table 3-1 of Peyrot (1978). The reported deflections appear to be based on an analysis assuming that all the members of the tower are tension-compression members. The X-braces in the lowest two panels of the tower are obviously intended to carry tension only. They are L1½x1½x3/16 (38.1 mm x 38.1 mm x 4.76 mm) angles with horizontal compression members bounding them. Table 4-3 compares

the reactions for a 9807 N (1000 kgf) load at the center of the top of the tower with the reactions for an analysis assuming these x-braces are tension-compression members and with an analysis assuming they are tension-only members. These analyses did not include the dead load of the tower. The tension-only members were modeled by using a modulus of elasticity in compression of 1/1000 the modulus in tension. Note that the longitudinal reactions are equal at all four legs for the tension-compression analysis but that more longitudinal load is carried by the back supports in the tension-only analysis.

**Table 4-3  
Reaction Comparison**

Location	Dir.	Reported (kN)	Adina T-C (kN)	Adina T-only (kN)
Ahead Left	L	-2.46	-2.45	-2.10
Adina Node 1	T	-3.95	-3.93	-2.81
Peyrot et al. B2	V	23.2	22.9	22.9
Back Left	L	-2.46	-2.45	-2.80
Adina Node 3	T	3.95	3.93	3.91
Peyrot et al. B1	V	-23.2	-22.9	-22.9
Back Right	L	-2.46	-2.45	-2.80
Adina Node 5	T	-3.95	-3.93	-3.91
Peyrot et al. B3	V	-23.2	-22.9	-22.9
Ahead Right	L	-2.46	-2.45	-2.10
Adina Node 7	T	3.95	3.93	2.81
Peyrot et al. B4	V	23.2	22.9	22.9

The deflections at key points are compared in Table 4-4.

**Table 4-4  
Deflection Comparison**

Location	Longitudinal Deflection due to 9.807 kN Longitudinal Load applied at Location		
	Reported (cm)	Adina T-C (cm)	Adina T-only (cm)
Center of Tower Top	1.90	1.85	1.90
Shield Wire Attachment Point	2.51	2.38	2.60
Upper Phase Attachment Point	2.88	2.64	3.08
Middle Phase Attachment Point	2.10	1.97	2.59
Lower Phase Attachment Point	0.97	0.89	1.33

In order to be able to reduce the number of nodes and members in the transmission line model, a dynamically similar model for the tower attachment point was constructed. A two-degree of freedom spring mass system is needed in the horizontal direction to model the combined longitudinal and torsional vibration characteristics of the tower and a single degree of freedom spring mass system is needed to model the vertical vibration characteristics. The horizontal and vertical spring stiffnesses should match the stiffnesses at the tower attachment point and the spring mass systems should have the same natural frequencies as the tower.

The static analyses also included load cases to determine the attachment stiffness in the vertical and longitudinal directions. The dead load of the tower was included in all load cases. The first load case was a longitudinal load of 9.807 kN (1000 kfg) applied at the top left phase attachment point to determine the overall deflection of the attachment point. The second case was two longitudinal loads of 4.9035 kN (500 kfg) applied at the two upper phase attachments. This case gives the longitudinal

deflection at the phase attachments without the torsional component of the deflection. In a separate load case, a 9.807 kN vertical load was applied to the attachment point to measure the vertical stiffness. These results are summarized in Table 4-5.

**Table 4-5  
Wisconsin Test Tower Deflections and Stiffnesses**

	Applied Longitudinal Load			Deflection (cm)	Stiffness (kN/m)
	Upper Left Phase (N)	Upper Right Phase (N)	Total (N)		
Total Deflection	9807.0	-	9807.0	3.138	313
Balanced Deflection	4903.5	4903.5	9807.0	1.437	682
Torsional Deflection	9807.0	-	9807.0	1.700	577

Analysis of the natural frequencies and mode shapes of the tower was also performed. The analysis was done for two cases, the first assuming that the tension-only cross bracing acted as tension-compression bracing and in the second, the modulus of elasticity of the tension-only members was assumed to be one-half the modulus of elasticity of steel. This simulated the stiffness of a tension-only system by giving the total stiffness of these members equal to the stiffness of one of them. Changing the modulus rather than the area keeps the same mass in the model. Table 4-6 compares the two.

**Table 4-6  
Wisconsin Test Tower Frequencies**

Mode No.	Description	Frequency (Hz)	
		Tension-Compression Bracing	Tension Only Bracing
1	1 <sup>st</sup> Transverse Mode	4.74	4.67
2	1 <sup>st</sup> Longitudinal Mode	4.79	4.72
3	1 <sup>st</sup> Torsional Mode	9.67	7.79

Note that there is very little difference in the 1<sup>st</sup> transverse and longitudinal modes. There is a significant difference in the frequency of the 1<sup>st</sup> torsional mode because the bracing is the main contributor to the torsional stiffness. Peyrot et al. (1978) reported a natural frequency by analysis of approximately 5 Hz, which is consistent with the frequencies reported in Table 4-6.

The natural frequencies of the ADINA Model were also explored by plucking the tower with a 20 kN force released in 0.005 s. This was applied in three directions, longitudinally with a 10° downdrop angle (x and -z), transversely (y) and vertically (-z). Figure 4-6 shows the Fourier analysis of the plucking loads (5 s duration of record). Table 4-7 compares the frequency analysis with the plucking analysis.

**Table 4-7**  
**Comparison of Frequency Analysis and Plucking Analysis**

Mode No.	Description	Frequency (Hz)	
		Frequency Analysis	Plucking Analysis
1	1 <sup>st</sup> Transverse Mode	4.67	4.60
2	1 <sup>st</sup> Longitudinal Mode	4.72	4.60
3	1 <sup>st</sup> Torsional Mode	7.79	7.2-7.4

Plucking the arm vertically excites the tower in the first transverse mode with a frequency of 4.6 Hz.

The longitudinal motion of the tower at the end of the crossarm is made up of a balanced longitudinal component and a torsional component requiring a two degree of freedom system of springs and masses to represent the longitudinal motion of the

tower. With its small relative amplitude, the vertical motion of the tower can be represented by a single degree of freedom spring-mass system.

Figure 4-7 shows the first longitudinal model considered. The global stiffness matrix is shown in Equation 4-1 and the mass matrix in equation 4-2.

$$k_g = \begin{bmatrix} k_1 + k_2 & -k_2 \\ -k_2 & k_2 \end{bmatrix} \quad \text{Equation 4-1}$$

$$m_g = \begin{bmatrix} m_1 & 0 \\ 0 & m_2 \end{bmatrix} \quad \text{Equation 4-2}$$

The natural frequencies are determined by solving the eigenproblem in Equation 4-4.

$$|k_g - \omega_n^2 m_g| = 0 \quad \text{Equation 4-3}$$

In this case, we know the natural frequencies and the stiffnesses and need to calculate the associated masses. Solving Equation 4-3 for the mass  $m_2$  in terms of mass  $m_1$  gives Equation 4-4.

$$m_2 = \frac{k_2 \omega^2 m_1 - k_1 k_2}{m_1 \omega^4 - (k_1 + k_2) \omega^2} \quad \text{Equation 4-4}$$

Using equation 4-4 but assuming two natural frequencies,  $\omega_1$  and  $\omega_2$ , gives Equation 4-5 which can be solved for  $m_1$  in terms of the spring stiffnesses and natural frequencies giving Equation 4-6.

$$m_2 = \frac{k_2 \omega_1^2 m_1 - k_1 k_2}{m_1 \omega_1^4 - (k_1 + k_2) \omega_1^2} = \frac{k_2 \omega_2^2 m_1 - k_1 k_2}{m_1 \omega_2^4 - (k_1 + k_2) \omega_2^2} \quad \text{Equation 4-5}$$

$$m_1^2 [k_2 \omega_1^2 \omega_2^2 (\omega_2^2 - \omega_1^2)] + m_1 [k_1 k_2 (\omega_1^4 - \omega_2^4)] + k_1 k_2 (k_1 + k_2) (\omega_2^2 - \omega_1^2) = 0 \quad \text{Eq. 4-6}$$

Equation 4-6 is a quadratic equation in  $m_1$ . For the solution to have physical sense, the mass must be positive and real. There may be no real positive root, one root or two roots. For the Wisconsin tower, Equation 4-6 has imaginary roots making the model shown in Figure 4-7 unsuitable for use in modeling the test line.

The tower can, however, be modeled with a different set of springs and masses. The balanced longitudinal mode of vibration is modeled as a linear translational spring-mass system. The torsional mode is modeled as a torsional spring with a rotational inertial mass. Both linear and torsional springs are connected to a rigid massless arm with length  $L$  equal to the horizontal distance from the center of the tower to the conductor attachment point as shown in Figure 4-8. The vertical motion of the tower is also modeled using a torsional spring with a rotational inertial mass as shown in Figure 4-8. The mass associated with the linear longitudinal spring was calculated using Equation 4-7.

$$m = \frac{k}{\omega_n^2} \quad \text{Equation 4-7}$$

The torsional spring constants and rotational moments of inertia were calculated using Equations 4-8 and 4-9 where  $P$  is the applied load and  $\delta$  is the resulting longitudinal deflection. The results are summarized in Table 4-8.

$$k_t = \frac{PL}{\arcsin\left(\frac{\delta}{L}\right)} \quad \text{Equation 4-8}$$

$$J = \frac{k_t}{\omega_n^2} \quad \text{Equation 4-9}$$

Damping for the linear and torsional spring-mass systems is calculated using equations 4-10 and 4-11, respectively.

$$c = 2\zeta m \omega_n \quad \text{Equation 4-10}$$

$$c_t = 2\zeta J \omega_n \quad \text{Equation 4-11}$$

Table 4-8 shows the properties of the equivalent spring-mass systems.

**Table 4-8**  
**Equivalent Mass, Stiffness and Damping**

	Frequency (Hz)	Natural Frequency (rad/s)	Stiffness (kN/m)	Associated Mass/ Rotational Inertial Mass (kg)	Damping 5% Critical (kg/s)
Longitudinal	4.60	28.9	682	817	2360
	(Hz)	(rad/s)	(kN-m/rad)	(kg-m <sup>2</sup> )	(kg-m <sup>2</sup> /s)
Torsional	7.20	45.2	8708	4255	19000
Vertical	4.60	28.9	17620	21100	61000

Figure 4-9 compares the time histories of the longitudinal displacements of the full tower model and the reduced tower model described above under a longitudinal plucking load that is inclined downwards at a 10° angle from horizontal. Figure 4-10 shows the Fourier spectra for the full and reduced tower models. The natural frequencies of the reduced tower model match very well with those of the full tower model.

## 4.5 Modeling the Conductor

### 4.5.1 Introduction

When a conductor breaks next to a suspension insulator and the insulator swings into the span, there are several aspects to the conductor response (Haro et al. 1956; Peyrot et al. 1978). These include a reduction in the static tension (the tension at rest after dynamic effects have damped out), an axial release wave which travels along the conductor, a transverse wave which is excited by the upward motion of the insulator string as it swings into the span and excitation of the natural vibration modes of the span by the fall of the wire.

#### 4.5.1.1 Axial Release Waves

The release wave travels down the conductor axis due to the sudden loss of tension. In the conductor, which is a taut string, this wave travels at approximately the speed of sound in the material as given in Equation 4-12 (Main 1978, p171) where  $E$  is the modulus of elasticity and  $\rho$  is the mass density of the material.

$$V_L = \sqrt{\frac{E}{\rho}} \quad \text{Equation 4-12}$$

The Ibis conductor used in the tests consists of a straight galvanized steel core wire with six galvanized steel wires wrapped around it in helices (see Figure 4-3). Over this seven strand steel cable, two layers of aluminum wires are also wound in helices. The diameter of the helices is larger in the outer layers. The release wave must travel slightly farther in each layer than in the layer below. Each layer, however, is bound to the adjacent layers by the friction between the strands which depends on the tension in the wire and whether the individual wires were preformed before stranding.

Rods with area  $A$  have a characteristic impedance  $Z_L$  to longitudinal waves as given in Equation 4-13 (Main 1978, p172) which has same units as viscous damping, kg/s.

$$Z_L = A \sqrt{E\rho} \tag{Equation 4-13}$$

Table 4-9 compares the speed of sound in aluminum and galvanized steel rods [properties from Thrash (1994, Table 1-1)] and in the completed conductor based on its composite density and modulus of elasticity (Alcoa 1974; Farr 1980). Also included for comparison is a 38.1 mm (1.5 in) diameter steel rod typical of a 100 kN canister load cell. The longitudinal wave velocities of the steel and aluminum rods are practically the same. It is reasonable to model the conductor as a solid bar with the final modulus of elasticity given in Table 4-9 (Farr 1980).

**Table Table 4-9  
Longitudinal Material Properties**

Description	Area (mm <sup>2</sup> )	Density (kg/m <sup>3</sup> )	Modulus Of Elasticity (GPa)	Longitudinal	
				Velocity (m/s)	Impedance (kg/s)
Aluminum Rod	7.74	2705	69.0	5051	106
Galvanized Steel Rod	4.68	7780	200.0	5070	185
Ibis Conductor	234.00	3476	74.2	4620	3758
100 kN Load Cell	1140.00	7820	200.0	5057	45100

**4.5.1.2 Transverse Waves**

The suspension insulator swings upward even while the conductor starts to fall. A portion of the motion of the conductor will be perpendicular to the conductor axis

generating a transverse wave that travels at the velocity given in Equation 4-14 (Main 1978, p139).

$$V_T = \sqrt{\frac{T}{m}} \quad \text{Equation 4-14}$$

The characteristic impedance to transverse waves is given in Equation 4-15 (Main 1978, p146). As with the longitudinal impedance, the units are those of viscous damping.

$$Z_T = \sqrt{T m} \quad \text{Equation 4-15}$$

#### 4.5.1.3 Changes in Impedance

At changes in the impedance, part of the wave is reflected and part transmitted. The amplitudes of the transmitted  $A_t$  and reflected waves  $A_r$  for a wave with amplitude  $A$  traveling in a conductor with impedance  $Z_1$  and encountering a change of impedance to  $Z_2$  are given in equations 4-16, (Main 1978, pp149-151). These equations apply to both transverse and longitudinal waves.

$$A_R = A \left( \frac{Z_1 - Z_2}{Z_1 + Z_2} \right) \quad A_T = A \left( \frac{2 Z_1}{Z_1 + Z_2} \right) \quad \text{Equation 4-16}$$

There is a large change in the transverse impedance at a suspension string, particularly for a downward wave where the entire mass of the insulator string and part of the tower must be accelerated. Most of the wave will be reflected; Buchanan (1934) reports reflected amplitudes of 92 to 98 percent of the incident amplitudes. This property is taken advantage of in sagging transmission and distribution lines by

the “return wave method” (RUS 1998). Similarly, one could expect reflections of longitudinal waves at the interface between the conductor and a load cell or the conductor and deadend.

#### **4.5.2 Natural Frequencies and Mode Shapes of Conductors**

Methods of calculating the natural frequencies of single spans of wire are described in Appendix A. One measure of the goodness of the finite element model of a structure is how well the natural frequencies calculated for the finite element model conform to the theory. A second measure is how the frequencies converge as the length of the elements is reduced. Table B-1 compares theoretical calculations of the natural frequencies of a typical 300 m span with the results of ADINA analyses for different numbers of elements in the span. There is little change in the natural frequencies for the higher modes when at least 60 elements are used and practically no difference between 120 elements and 300 elements. Based on the results in Table B-1, the length of the wire elements was chosen to be approximately 2.5 m. Each span was broken into the number of equal length elements closest to 2.5 m.

#### **4.5.3 Conductor Damping**

Damping of transmission conductors can be separated into internal damping and aerodynamic damping. The internal damping is a combination of hysteretic damping within the individual cable strands and damping due to the sliding friction between strands as they move past one another during cable movement. Aerodynamic damping arises from the motion of the cable through the air.

Much of the literature related to the damping of transmission conductors is focused on the energy dissipated by the cable when excited by vortex shedding in smooth laminar winds. This motion is known as aeolian vibration. The results of tests of the self-damping capabilities of the conductor are usually stated in terms of the energy dissipated per unit length as a function of the vibration frequency. The peak to peak amplitude of vibration is very small, typically less than the conductor diameter (Gilbert/Commonwealth 1979, p 3). These measurements often do not distinguish between the internal damping and the aerodynamic damping, in some cases describing the vortex excitation as *negative aerodynamic damping*. The internal damping due to friction between the strands is reduced as the tension in the wire increases, and increases as the amplitude of vibration increases. Diana et al. (2000) indicate that the damping coefficient for ACSR conductor is in the range of 0.1 to 0.01 percent of critical for the frequencies and amplitudes of interest for aeolian vibration. Carne (Carne 1980) in discussing guys for vertical axis wind turbines reports damping of less than 0.2 percent of critical. In Bachmann et al. (1995, p 96) a value of 0.05 percent of critical is suggested.

#### **4.5.3.1 Internal Damping**

The internal damping can be divided into two parts, axial damping that takes place due to changes in the conductor tension, and lateral damping due to bending of the conductor. The critical axial viscous damping for a rod is given in Equation 4-17.

$$c_{cr} = 2\sqrt{AEm}$$

Equation 4-17

Note that the critical damping constant is independent of the length of the rod. Table 4-10 shows some values of axial damping used in previous time history analyses of conductor motion. McClure and Tinawi (1989a; 1989b) did not use explicit damping, however some of the time history analysis algorithms they investigated introduce some numerical damping.

**Table 4-10  
Axial Damping Ratios**

Reference	Description	Axial Damping Ratios % Critical
Thomas (1981)	Broken Wire Analysis	5 to 20%
McClure & Tinawi (1989a; 1989b)	Broken Wire Analysis	0% (see text)
Roshan-Fekr (1995)	Ice Shedding Analysis Bare Conductor	2%
	Iced Conductor	10%
McClure & Lapointe (2003)	Broken Wire Analysis Bare Conductor	2%
	Iced Conductor	10%

Little information seems to be available on the lateral damping of ACSR conductor; however, Yu (1952) presents results of some tests performed on slack steel cables similar to those used for shield wires and the steel core of ACSR. These tests indicate there may be substantial lateral damping.

#### 4.5.3.2 Aerodynamic Damping

ADINA has the capability of modeling the aerodynamic damping directly. Aerodynamic damping is due to the motion of the conductor relative to the air. In

still air the aerodynamic damping is given by Equation 4-18 (Dyrbye and Hansen 1996, p. 76).

$$F_d = \frac{1}{2} \rho V_r^2 C_d A \quad \text{Equation 4-18}$$

Where  $F_d$  is the damping force,  $\rho$  is the air density and  $V_r$  is the velocity relative to the air,  $C_d$  is the drag coefficient and  $A$  is the projected area.  $C_d$  depends on the Reynolds number (Equation 4-19) where  $d$  is the conductor diameter and  $\mu$  is the viscosity of air.

$$Re = \frac{\rho V_r d}{\mu} \quad \text{Equation 4-19}$$

For smooth circular cylinders,  $C_d$  is between approximately 0.9 and 1.2 for Reynolds numbers between 200 and 100,000 (Binder 1973; Eisner 1931), which correspond to relative velocities for Ibis conductor of 0.15 m/s and 73 m/s, respectively. As the relative velocity is reduced below a Reynolds number of 200,  $C_d$  steadily increases to over 50 at a Reynolds number of 0.1. A  $C_d$  of 1.25 was used for the initial calculations.

#### 4.5.3.3 ADINA Conductor Model

Figure 4-11 shows the basic conductor model used in ADINA with both axial and aerodynamic damping. Although the aerodynamic damping should be applied normal to the direction of movement, this would be more difficult to model in ADINA. Instead, the aerodynamic damping was applied to the vertical motion of the conductor using the initial horizontal projected area.

## 4.6 Modeling of the Insulator Assemblies

In the instrumented insulator string at tower T3, the porcelain insulators were replaced with a section of wire rope and a Dillon 10,000 lb (44.5 kN) load cell. At tower T4, a load cell was also included; however, the film (EPRI 1978) shows four porcelain insulator bells left in the string. The remaining towers are assumed to have the original insulator strings. No information is included in the test report on the connections, dimensions and properties of the load cells and wire rope.

The wire rope is assumed to be 16 mm (5/8 in) improved plow steel with 6x19 fiber core stranding. The area is  $103 \text{ mm}^2$  ( $0.16 \text{ in}^2$ ); after prestressing, the modulus of elasticity is 82.7 GPa (12,000 psi) for loads between 21% and 65% of the rated tensile strength of 149 kN (16.7 U.S. tons) (Wire Rope Technical Board 1993).

Based on information in the current Dillon Catalog (Dillon 1998), the load cells are estimated to be constructed of steel with a diameter of 34.9 mm (1.375 in). The length used in the model includes an allowance for hardware to connect the load cells to the conductor clamp and the wire rope.

The swinging brackets and insulators are modeled as 15.875 mm (0.625 in) steel rods.

Lumped masses are added at nodes in the model to get the same total mass and approximately the same mass distribution as the test components. Figure 4-12 shows a complete insulator assembly and the three insulator models used in the analysis.

#### **4.7 Time History Analysis Results**

Figure 4-13 shows the load cell tension at tower T3 from a time history analysis of test III L3 performed with ADINA (ADINA 2001). A summary of the parameters used in the ADINA model is given in Appendix B. Also shown in Figure 4-13 is the load cell tension from Peyrot et. al. (1978).

Figures 4-14 & 4-15 show the Fourier transforms of both the ADINA time history and the test record for test III L3. The amplitudes of frequencies above 8 to 10 Hz in the test record are very small in comparison to the amplitudes from the ADINA Model. An inverse Fourier transform of only the frequencies below 10 Hz in the test record could not be distinguished from the original, while higher frequencies are obviously represented in the ADINA time history.

The test report indicates (page 5-1) that "...the basic concern for the instrumentation was within the low frequency to DC range for the basic vibrational characteristics." The fundamental frequency of the tower was expected to be in the neighborhood of 5 Hz. The load cell signals were conditioned before recording with an oscillographic recorder. No detail is given about the extent of the signal conditioning; however, it is likely that a low pass analog filter was used to eliminate 60 Hz noise. Note that, even

though higher frequencies would be expected in model tests, Kempner (1997) used a low pass filter with a 50 Hz cutoff in his model tests. Note also that analog low pass filters partially attenuate some of the frequencies below the nominal cutoff frequency. It can be reasonably inferred that any higher frequencies as shown in Figure 4-15 would, if they occurred in the tests, have been filtered out or attenuated before recording the data.

The ADINA time history analysis can itself be expected to introduce some higher frequencies in the response due to breaking up the continuous elements in the real structure into discrete pieces in the finite element model. In some past studies, damping has been increased to suppress these spurious frequencies in transmission line dynamic analysis (Roshan Fekr 1995). Holmes and Belytschko (1976) discuss the problem in reference to wave propagation problems and explore the use of digital filters to remove the spurious frequencies. Using unequal elements in the mesh will also introduce spurious frequencies due to reflections between elements (Bazant 1978). For this reason, using equal length elements to model the conductor is preferred. For convenience in calculation, lengths were made equal in the horizontal projection of the elements leading to small differences in the lengths within a span. Because spans must be divided up into an integral number of elements, there are also small differences in the length of elements used in the different spans. Some of the high frequency content shown in Figure 4-15 can reasonably be attributed to the modeling.

Digital filtering of the load cell tensions from the ADINA time history analysis is an effective way to remove the high frequency components for a better comparison with the full scale test data. Figure 4-16 shows the use of a 10 Hz low pass notch filter. A notch filter was used because it is extremely easy to program once the Fourier coefficients have been determined. Figure 4-17 compares 10 and 15 Hz notch filters. A 10 Hz notch filter was used for subsequent time history analyses.

Figures 4-18 to 4-20 compare the filtered results of the time history analyses for tests III L1, 2 and 3. In all three cases, there is a very good fit in the timing, the rise in tension and the peak tension of the first peak. The unloading part of the first peak does not have such a good fit. It appears to improve with the lower conductor tensions in tests III L2 and III L1. The small bumps on the rising part of the first peak may be explained by the bolted connections suddenly slipping during the loading cycle. Similarly the much faster reduction in tension during the fall of the first peak may be explained by permanent set in the tower caused by connections slipping. In a theoretical analysis of bolt slippage in the connections of lattice towers, Kitipornchai et. al. (1994) report an increase in deflection of 20 percent due to slippage in the connections.

The timing of second peak due to bottoming out of the fall of the first span of conductor is well predicted, but all three models substantially over-predict the magnitude of the peak. There is a small angle in line at tower T4 ( $1^{\circ} 31'$ ) which was not included in the ADINA model, this may explain some of the difference.

Increased movement of the tower under the impact due to slippage in the connections may also contribute to the difference.

Table 4-11 shows the magnitudes of the first and second peaks from the test. The magnitudes of the first peak follow in the order of the horizontal tension. The magnitudes of the 2<sup>nd</sup> peak in the tests are out of order with the Test III L3 less than Test III L2. As can be seen in Figure 4-21, the magnitudes of both peaks in the ADINA model are in order of horizontal tension. Unfortunately, there were no other successful tests with three tensions to indicate whether this is a problem with the tests or with the ADINA model.

**Table 4-11  
Peak Test Magnitudes**

Test No.	Horizontal Tension (kN)	1 <sup>st</sup> Peak (kN)	2 <sup>nd</sup> Peak (kN)
III L1	12.43	14.96	20.27
III L2	17.77	20.27	24.61
III L3	21.32	24.61	21.72

#### 4.7.1 Variations in the Model Parameters

Due to the discrepancy in the magnitudes of the second peaks from the tests, some variations in the model parameters were made to see the effects on the results.

Changing the modulus of elasticity of the wire rope in the insulator assemblies of towers T2 and T3 from 82.7 GPa to 41.35 GPa. (a 50% change) did not significantly affect the results.

The reduced tower model at tower T3 was replaced with the full tower model without any damping applied to the tower. There was no significant change in the results.

Changing the longitudinal and torsional natural frequencies of the towers from 4.6 to 4.0 and 7.2 to 6.6 Hz, respectively, by reducing the stiffness of the springs had only a minor effect on the results.

Changing the modulus of elasticity of the conductor from 74.2 GPa to 81.62 GPa had no significant effect on the magnitude and timing of the first two peaks; however, it made a noticeable difference after the second peak.

The effect of changing the insulator string lengths by changing only the length of the top element by 15 cm plus and minus (with no change in mass) is shown in Figure 4-22. The uncertainty in the insulator string length discussed above does not explain the difference between tests and ADINA models for the second peak

Some model runs were made with the span between towers T3 and T4 changed to 279 m due to the discrepancy noted above. This did not improve the fit with the test data. Rayleigh damping was tried, also without significant improvement. However, one run made with the 279 m span is of interest. The axial and aerodynamic dampers were replaced with grounded vertical viscous dampers giving damping vertically of 3.2 kg/s-m. The longitudinal spring constant of the tower was reduced to 516 kN/m

and the damping constant was increased to 2875 kg/s. This changed the longitudinal natural frequency of the tower from 4.6 Hz to 4.0 Hz and the damping ratio from 5 to 7 percent. The changes in the tower stiffness and damping were not significant, however, the change to the wire damping was. Figure 4-23 compares this damping with the original test data. The timing of the first peak is still good, but it is somewhat smaller in magnitude. The timing of the second peak is delayed, but the magnitude matches very well.

## **4.8 Conclusions**

Analog time histories from older test can be digitized and analyzed for their frequency content.

Digital Filtering is an effective way to remove the high frequencies introduced by breaking continuous systems up into a finite element model.

The ADINA time history analysis does a good job of predicting the first peak due to loss of conductor tension but a relatively poor job of predicting the magnitude of the second peak due to the retensioning of the conductor at the bottom of its fall. For the purposes of the proposed research, the model is adequate. The first peak is well modeled. The second peak is on the conservative side for evaluating the effect of measures introduced into the tower and insulator system to control impact.

The poor fit between the analytic results and the tests after the first peak shows that there is still work to be done in modeling conductor. Questions that need to be answered include: whether the bending stiffness of the conductor needs to be taken into account, and the type of damping and its application that best represent the physics of the conductor and its motion in the transient phase of the response when the peaks that need mitigation occur.

#### **4.9 Recommendations for Future Tests**

While the documentation for these tests is the best that is currently available in the literature, there are a few things that were not done in these tests that would help in modeling future tests. When tests are made on double circuit towers or the outside phase of single circuit towers, in addition to the longitudinal natural frequency, the torsional natural frequency of the tower should be determined. Accurate measurements of the static deflections of the tower for both balanced and torsional longitudinal loads including any permanent set should be determined experimentally to give a measure of the effects of the foundation stiffness and bolt slippage. Permanent set of the tower after the application of each broken wire load should be determined. Accelerometers placed at the center of the tower and at the insulator attachment point would allow the actual tower movement to be compared directly to the tower model.

Experimental measurements are usually filtered in some fashion before being recorded. Finite element models also introduce noise because systems that are

continuous in nature are broken up into discrete elements for analysis. As can be seen in Figure 4-16, the finite element results can also be filtered to remove some of the noise due to the model's discretization of a continuous structure. Knowing the filtering used in the physical measurements will allow similar filtering of the results from the finite element model, which should provide a better comparison between the measurements and the results of the finite element analysis.

The stress-strain relationship of new transmission conductor is highly nonlinear. The stress-strain characteristics of a conductor that has been in service are dependent on the installation technique and the in-service load history. If possible, the conductor properties: unit mass, area and modulus of elasticity, should be measured experimentally both before and after the tests.

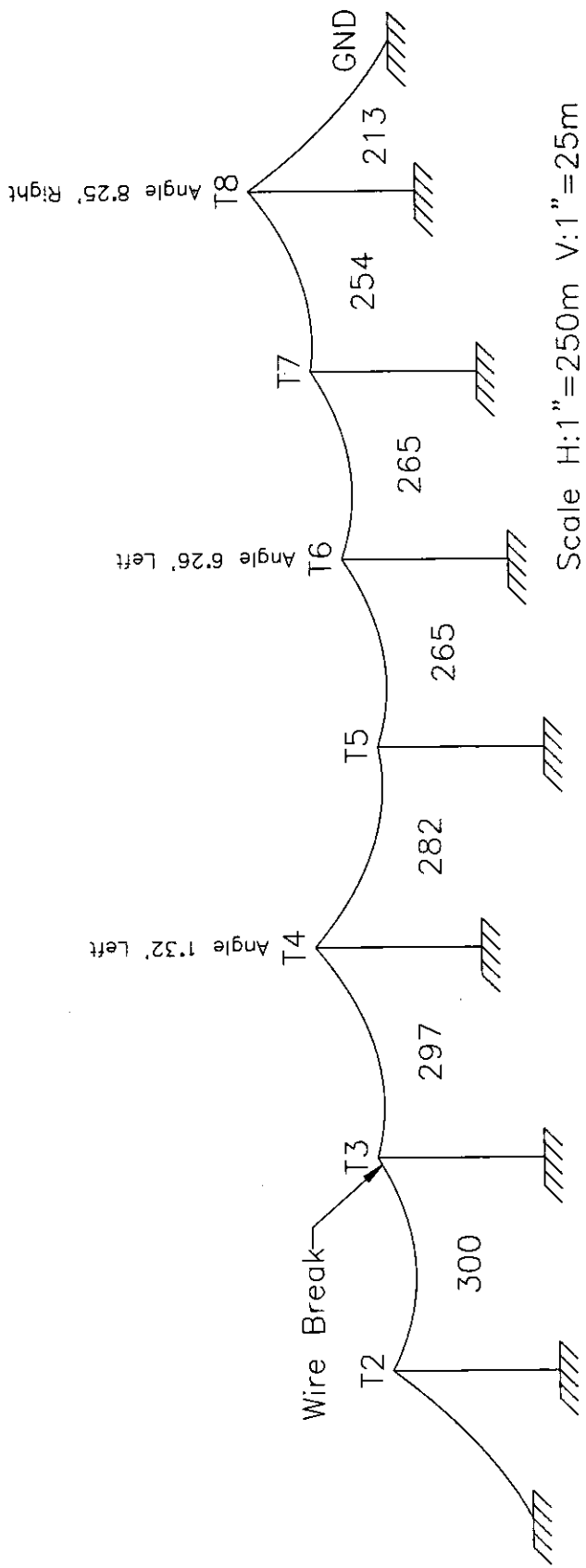
The wire movement at the quarter points in the span should be recorded if possible. Analyzing the movement at these three points for both frequency and phase could allow separation of the effects of traveling waves and excitation of the span in its normal modes.

More testing is needed to determine the lateral damping properties of transmission conductors.

## References

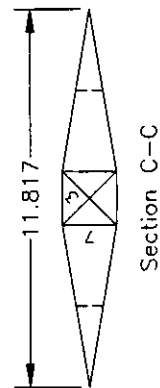
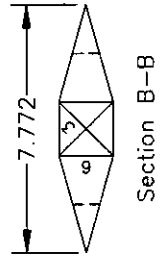
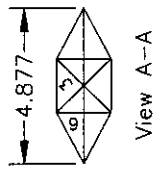
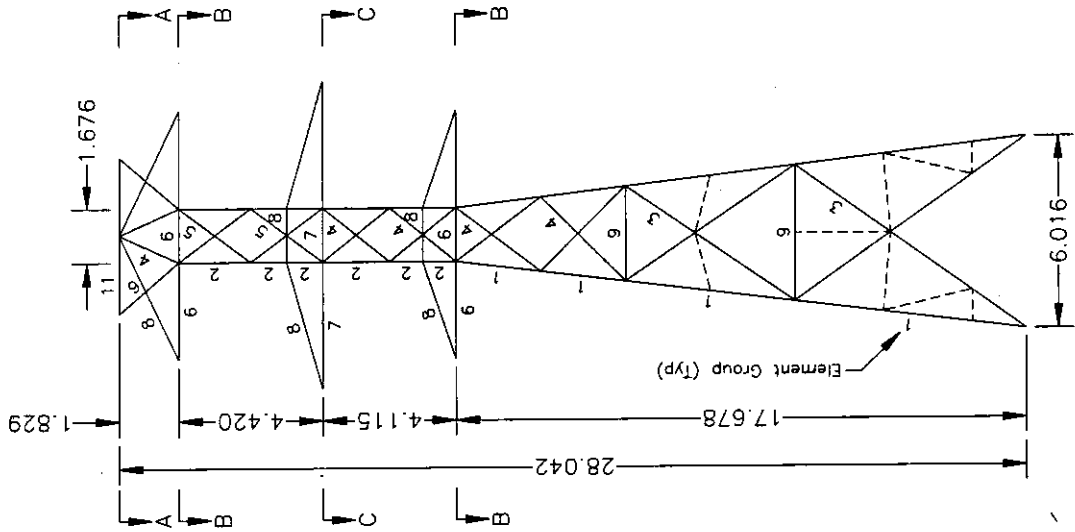
- ADINA (Automatic Dynamic Incremental Nonlinear Analysis). (2001). Version 7.5. ADINA R&D, Inc., Watertown, MA.
- Alcoa. (1974). *Product Data; Aluminum Electrical Conductors: Stranded-Bare, Covered Line Wire and Multiplex Cables; General Index*, Alcoa Conductor Products Company, Pittsburgh, PA.
- Bachmann, H., Amman, W. J., Deischl, F., Eisenmann, J., Floegl, I., Hirsch, G. H., Klein, G. K., Lande, G. J., Mahrenholtz, O., Natke, H. G., Nussbaumer, H., Pretlove, A. J., Rainer, J. H., Saemann, E.-U., and Steinbeisser, L. (1995). *Vibration Problems in Structures: Practical Guidelines*, Birkhauser Verlag, Basel and Boston.
- Bazant, Z. P. (1978). "Spurious Reflection of Elastic Waves in Nonuniform Element Grids." *Computer Methods in Applied Mechanics and Engineering*, 16(1), 91-100.
- Binder, R. C. (1973). *Fluid Mechanics, Fifth Edition*, Prentice-Hall, Inc., Englewood Cliffs, NJ.
- Buchanan, W. B. (1934). "Vibration Analysis-Transmission Line Conductors." *Transactions of the AIEE*, 53, 1478-1485.
- Carne, T. G. (1980). "Guy Cable Design and Damping for Vertical Axis Wind Turbines." SAND80-2669, Sandia National Laboratories, Albuquerque, NM.
- Diana, G., Falco, M., Cigada, A., and Manenti, A. (2000). "On the Measurement of Over Head Transmission Lines Conductor Self-Damping." *IEEE Transactions on Power Delivery*, 15(1), 285-292.
- Dillon. (1998). *Dillon Strain Gauge Loadcells, Bulletin #500.7*, Dillon Force Measurement Products and Systems Division of Weigh-Tronix, Inc., Fairmont, MN.
- Dyrbye, C. s., and Hansen, S. O. (1996). *Wind Loads on Structures*, John Wiley & Sons, Ltd, Chichester, GB.
- Eisner, F. (1931). Das Widerstandsproblem. In *Proceedings of the 3rd International Congress for Applied Mechanics, Stockholm 24-29 August 1930*, edited by C. W. Oseen and W. Weibull. AB. Sveriges Litografiska Tryckerier. Stockholm.
- EPRI. (1978). "Film of Longitudinal Loading Test on a Transmission Line, Madison Wisconsin, December 1977. EPRI Project 1096-1." Electric Power Research Institute.
- Farr, H. H. (1980). *Transmission Line Design Manual*, United States Government Printing Office, Denver, CO.
- Gilbert/Commonwealth. (1979). *Transmission Line Reference Book: Wind-Induced Conductor Motion*, Electric Power Research Institute, Palo Alto, Calif.
- Haro, L., Magnusson, B., and Ponni, K. (1956) "Investigations on Forces Acting on a Support after Conductor Breakage." *International Conference on Large Electric Systems (CIGRE)*, Paris, Report 210.
- Holmes, N., and Belytschko, T. (1976). "Postprocessing of Finite Element Transient Response Calculations by Digital Filters." *Computers and Structures*, 6, 211-216.

- Kempner, L. J. (1997). "Longitudinal Impact Loading on Electrical Transmission Line Towers: A Scale Model Study," Ph.D. Thesis, Systems Science : Civil Engineering, Portland State University, Portland, Oregon.
- Kitipornchai, S., Al-Bermani, F. G. A., and Peyrot, A. H. (1994). "Effect of Bolt Slippage on Ultimate Behavior of Lattice Structures." *Journal of Structural Engineering*, 120(8), 2281-2287.
- Kluge, R. O. 2002. Comments on EPRI Wisconsin Tests (Private correspondence), June.
- Main, I. G. (1978). *Vibrations and Waves in Physics*, Cambridge University Press, Cambridge.
- McClure, G., and Lapointe, M. (2003). "Modeling the Structural Dynamic Response of Overhead Transmission Lines." *Computers and Structures*, (In press: Paper No. 3070).
- McClure, G., and Tinawi, R. (1989a). "Comportement dynamique des lignes aériennes de transport d'électricité dû aux bris de câbles. I. Modélisation mathématique. (Dynamic Behavior of Overhead Electric Transmission Lines Due to Broken Cables. I Mathematical Modeling)." *Canadian Journal of Civil Engineering*, 16(3), 335-353.
- McClure, G., and Tinawi, R. (1989b). "Comportement dynamique des lignes aériennes de transport d'électricité dû aux bris de câbles. II. Problèmes numériques associés à la modélisation mathématique. (Dynamic Behavior of Overhead Electric Transmission Lines Due to Broken Cables. II Numerical Problems Associated with the Mathematical Modeling)." *Canadian Journal of Civil Engineering*, 16(3), 354-374.
- Peyrot, A. H., Kluge, R. O., and Lee, J. W. (1978). "Longitudinal Loading Tests on a Transmission Line." EPRI EL-905, Electric Power Research Institute, Palo Alto, CA.
- Roshan Fekr, M. (1995). "Dynamic Response of Overhead Transmission Lines to Ice Shedding," M.Eng. Thesis, Civil Engineering and Applied Mechanics, McGill University, Montreal, Quebec.
- RUS. (1998). *Bulletin 1726C-115, Checking Sag in a Conductor by the Return Wave Method*, USDA Rural Utilities Service, Washington, D.C.
- Thomas, M. B. (1981). "Broken Conductor Loads on Transmission Line Structures," Ph.D. Thesis, Civil and Environmental Engineering, The University of Wisconsin - Madison, Madison, Wisconsin.
- Thrash, R., Hudson, G., Cooper, D., and Sanders, G., eds. 1994. *Overhead Conductor Manual*. Carrollton, Georgia: Southwire Company.
- Wire Rope Technical Board. (1993). *Wire Rope Users Manual*, Wire Rope Technical Board, Woodstock, MD.
- Yu, A.-T. (1952). "Vibration Damping of Stranded Cable." *Experimental Stress Analysis*, 9(2), 141-158.



EPRI Wisconsin Test Line Profile

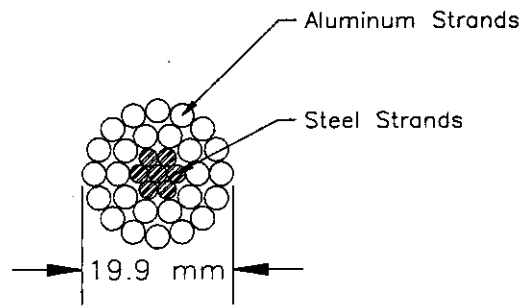
Figure 4-1



Element Group	Member Size
1	L5x5x5/16
2	L3½x3½x¼
3	L1½x1½x3/16
4	L2½x2½x3/16
5	L2½x2x3/16
6	L3½x3½x3/16
7	L4x3x¼
8	L2x2x3/16
9	L3x3x3/16
10	Dummy
11	2L3x2½x3/16

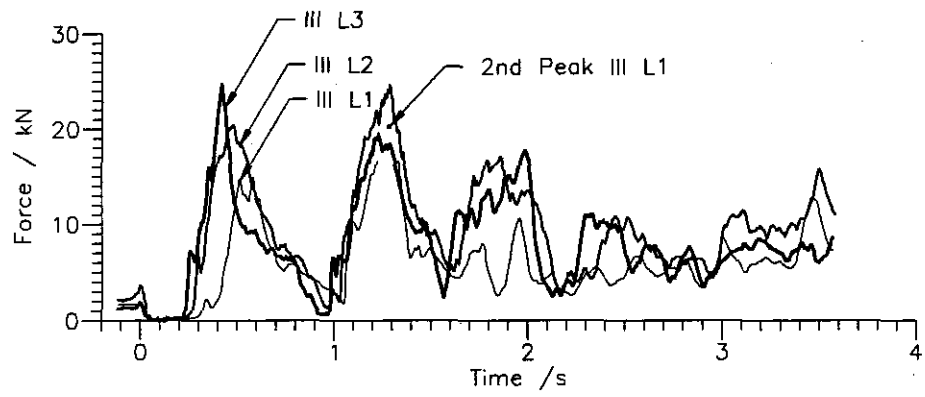
Notes:  
 Angles are U.S. sizes in inches  
 Tower Dimensions are in meters

Figure 4-2  
 Wisconsin Test Towers



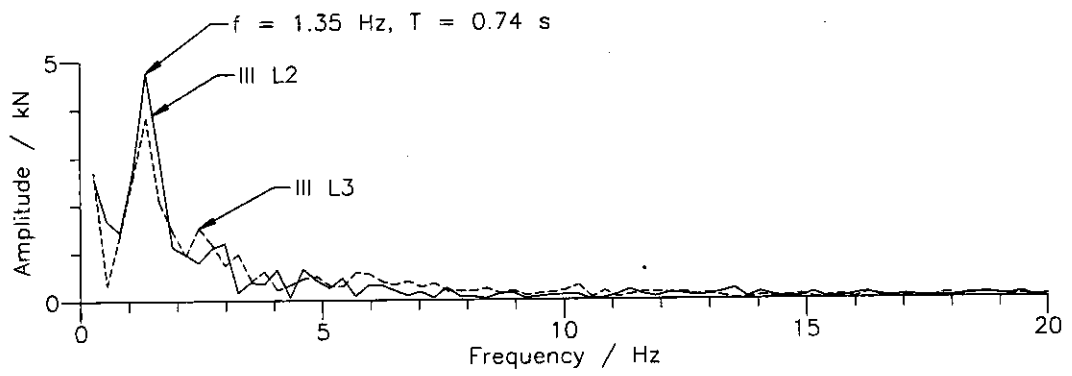
Ibis Conductor

Figure 4-3



Insulator Tension at Tower T3  
Tests III L 1, 2 & 3

Figure 4-4



Fourier Spectra  
Wisconsin Tests III L2 & 3

Figure 4-5

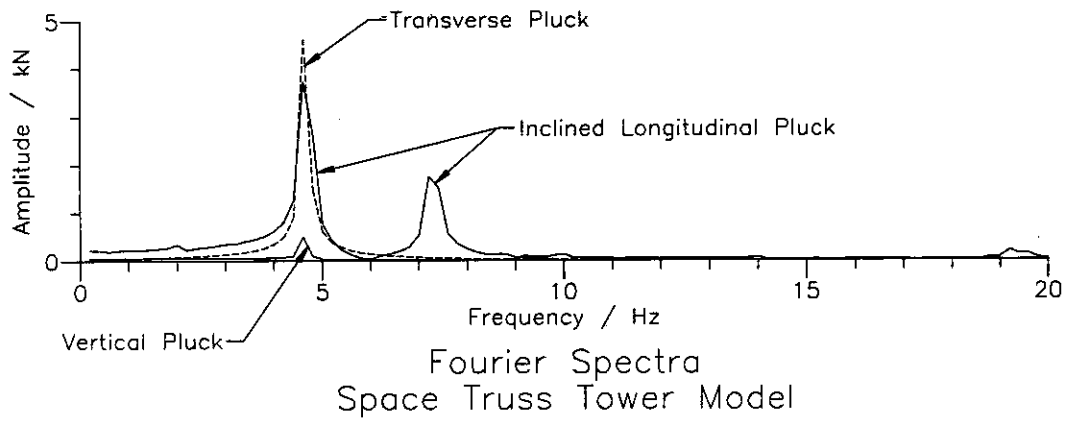
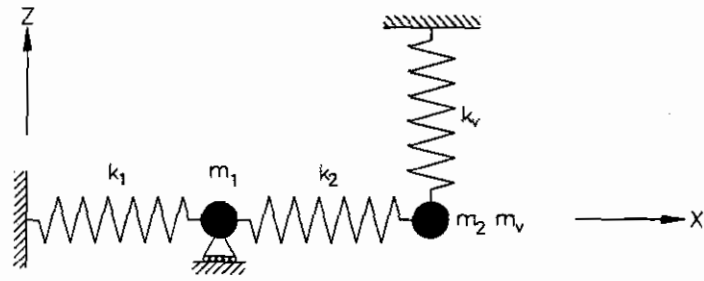


Figure 4-6



Linear 2 DOF Spring-Mass System

Figure 4-7

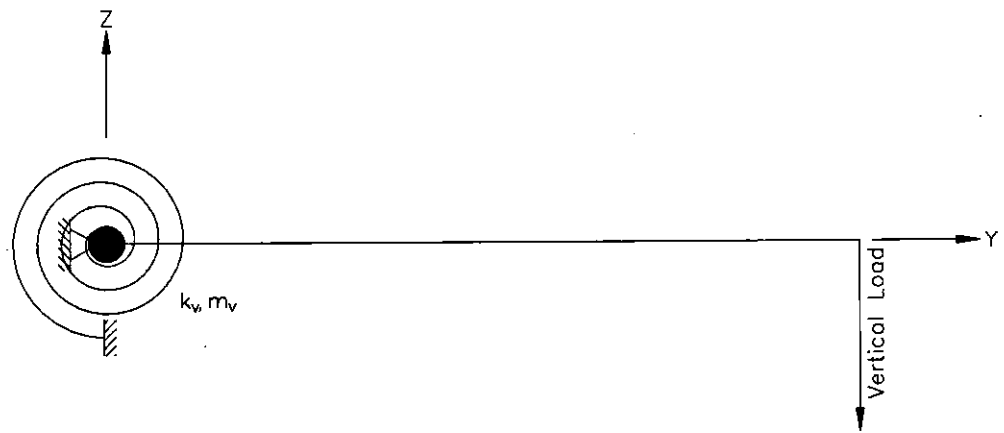
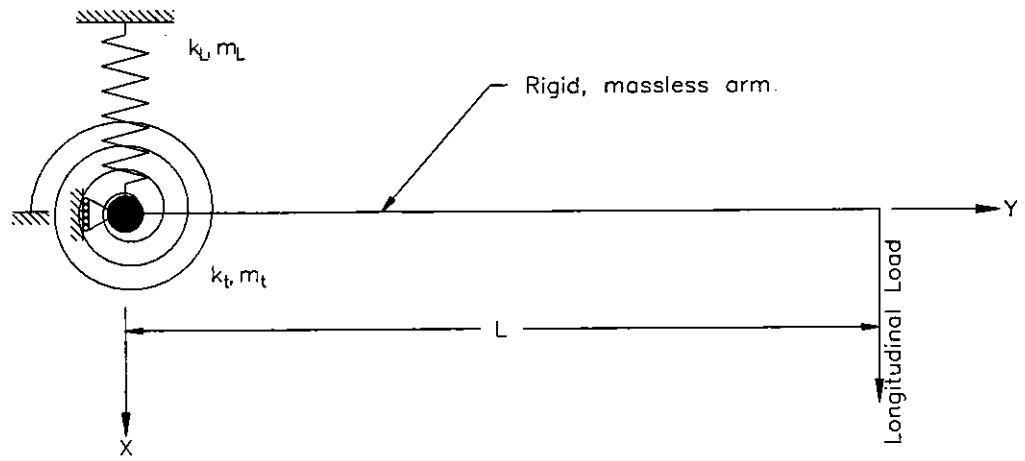
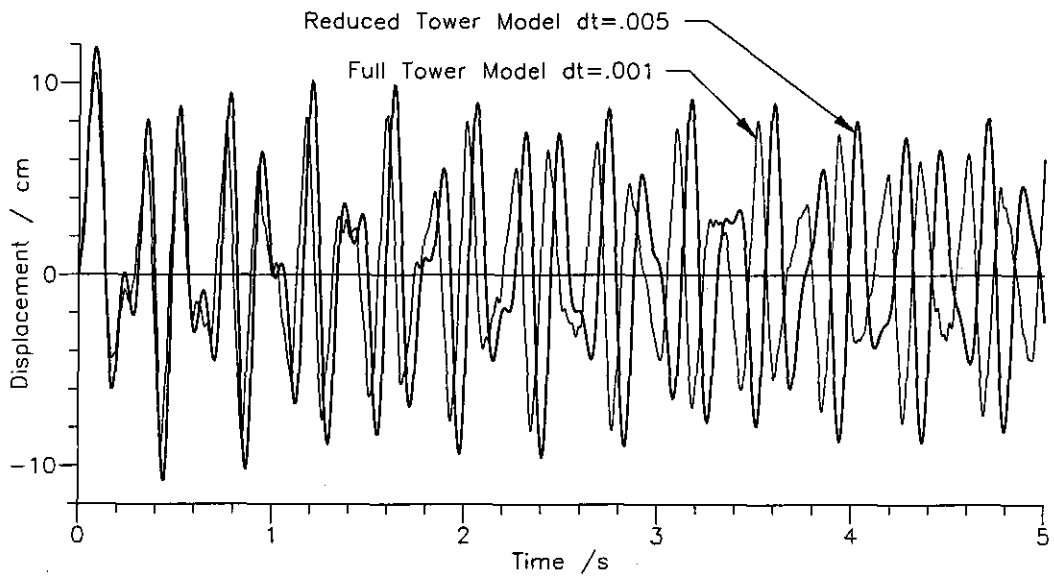
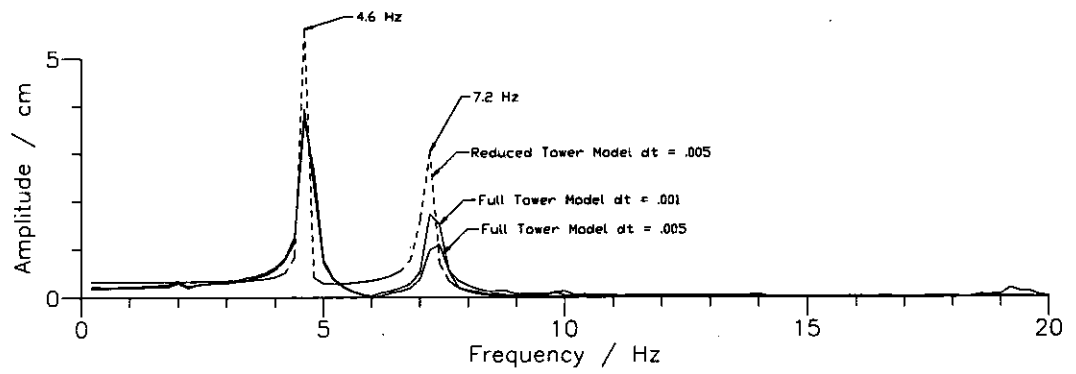


Figure 4-8  
Wisconsin Tests  
Reduced Tower Model



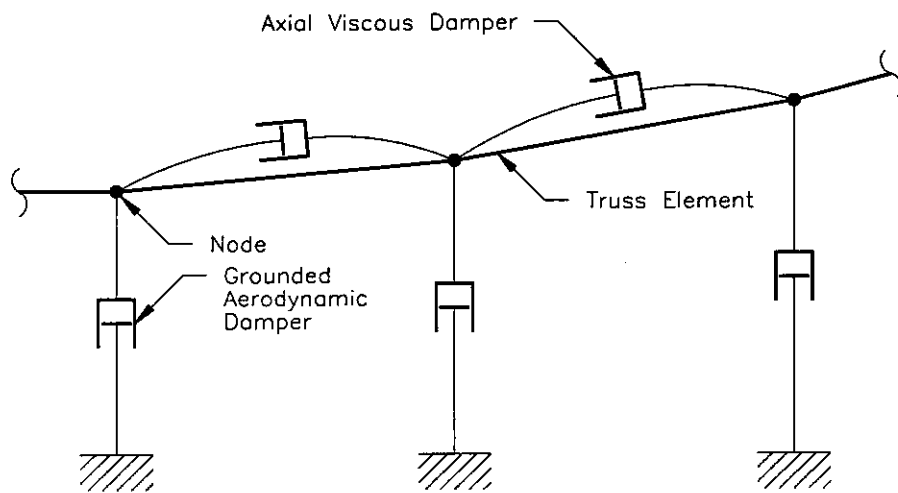
Longitudinal Deflection at Upper Left Phase  
Comparison of Full and Reduced Tower Models

Figure 4-9



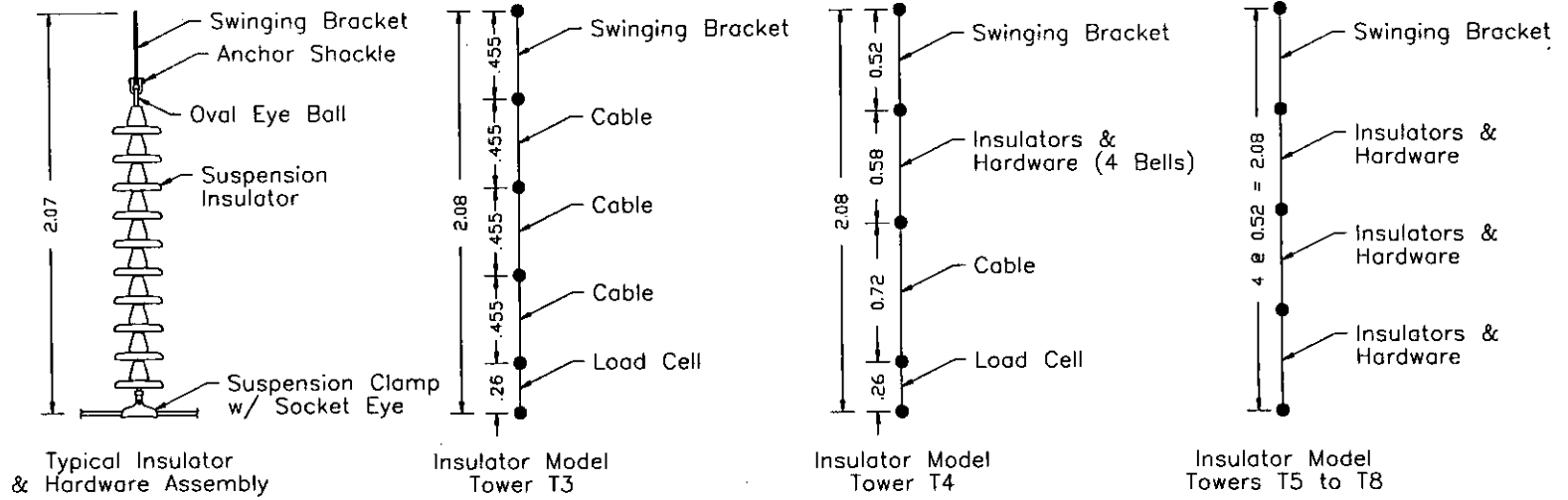
Fourier Spectra  
Tower Model Comparison

Figure 4-10



Conductor Model

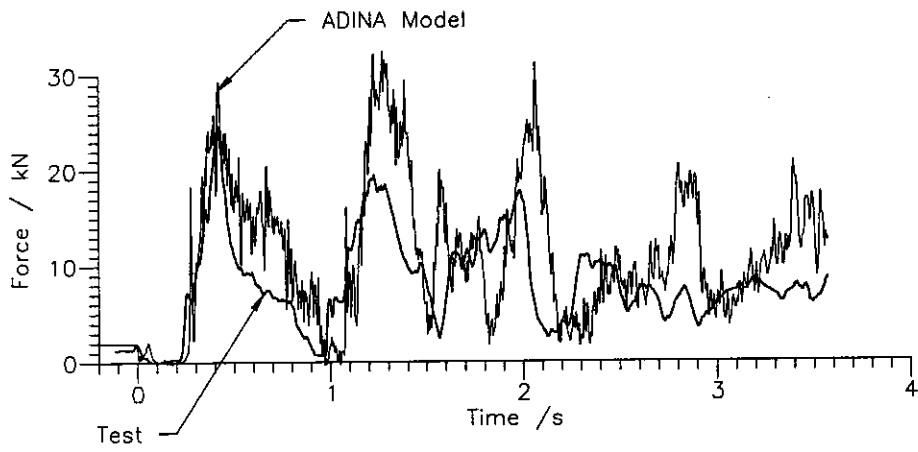
Figure 4-11



Note: All Dimensions in meters

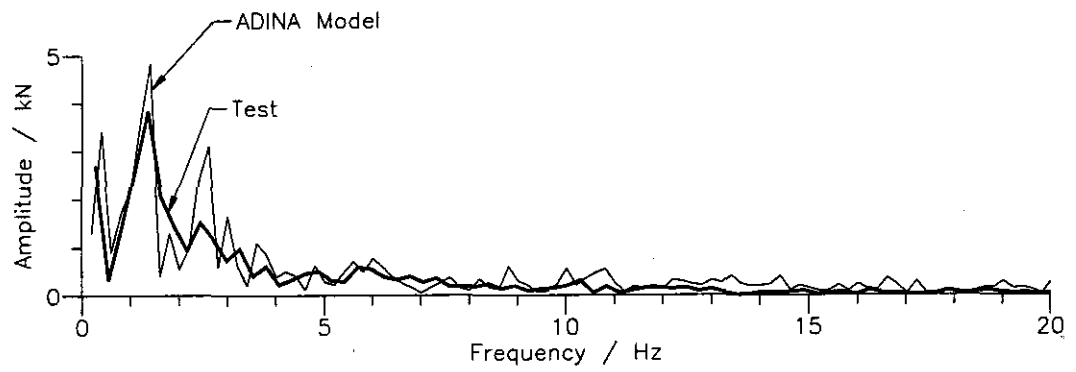
Insulator & Hardware Assembly Models

Figure 4-12



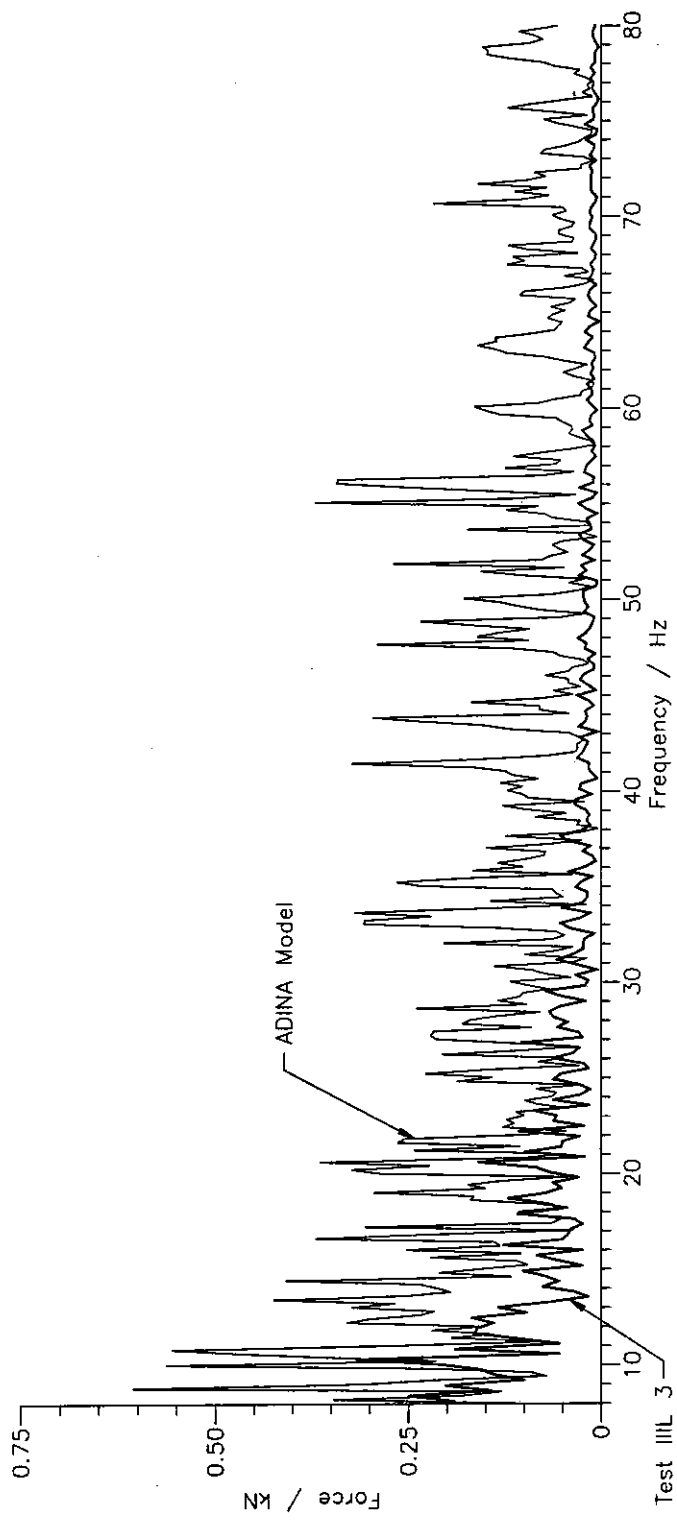
Insulator Tension at Tower T3  
Test III L3 vs ADINA Model

Figure 4-13



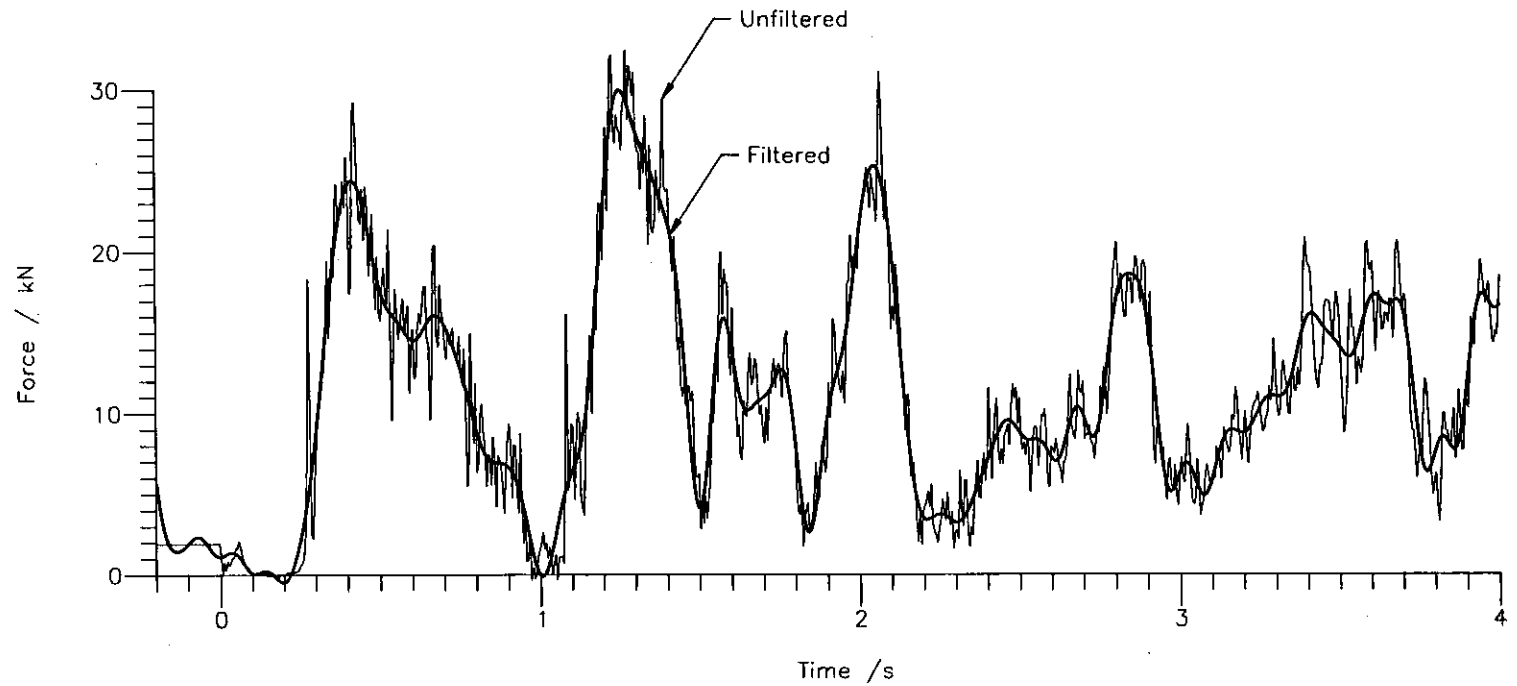
Frequency Content  
Test III L3 and ADINA Model

Figure 4-14



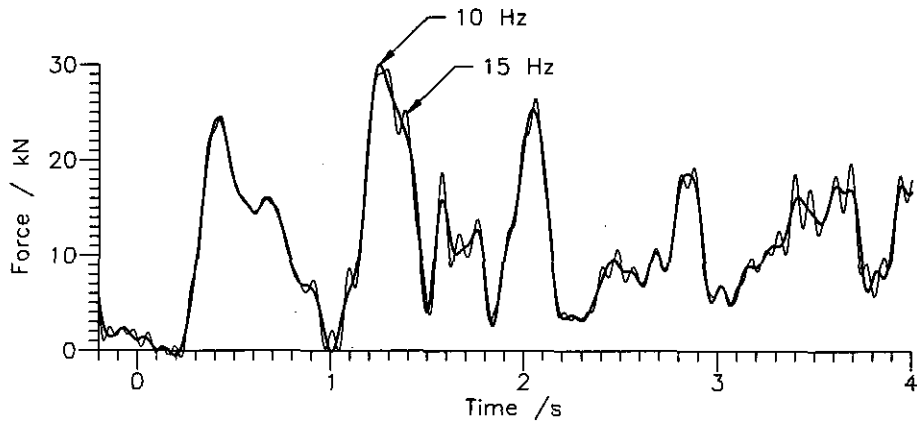
High Frequency Content of Test III L3 and ADINA Model

Figure 4--15



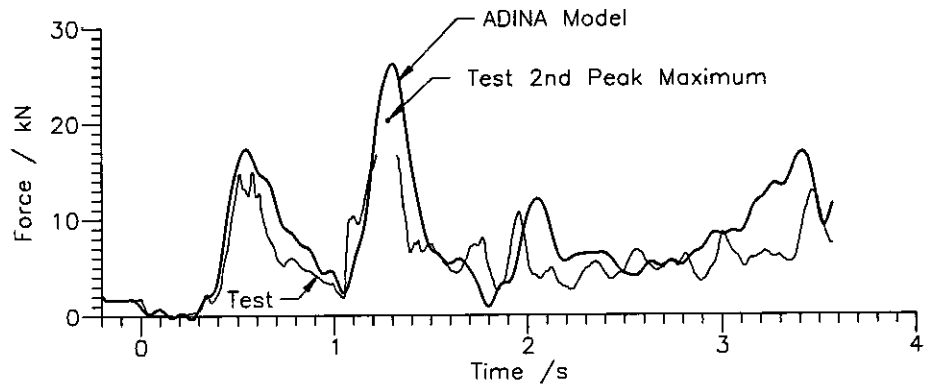
Insulator Tension at Tower T3, Test III L3  
ADINA Model vs ADINA Model with 10 Hz Low Pass Notch Filter

Figure 4-16

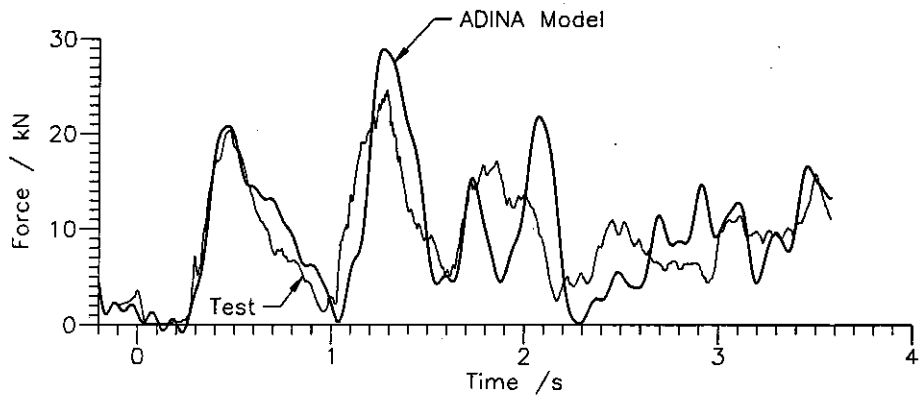


Insulator Tension at Tower T3, Test III L3  
Comparison of 10 Hz and 15 Hz Low Pass Notch Filters

Figure 4-17

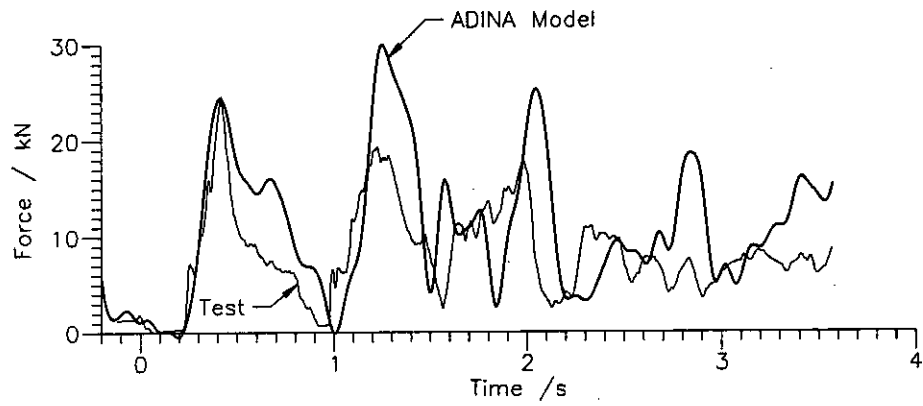


Insulator Tension at Tower T3  
Test III L1 vs Filtered ADINA Model



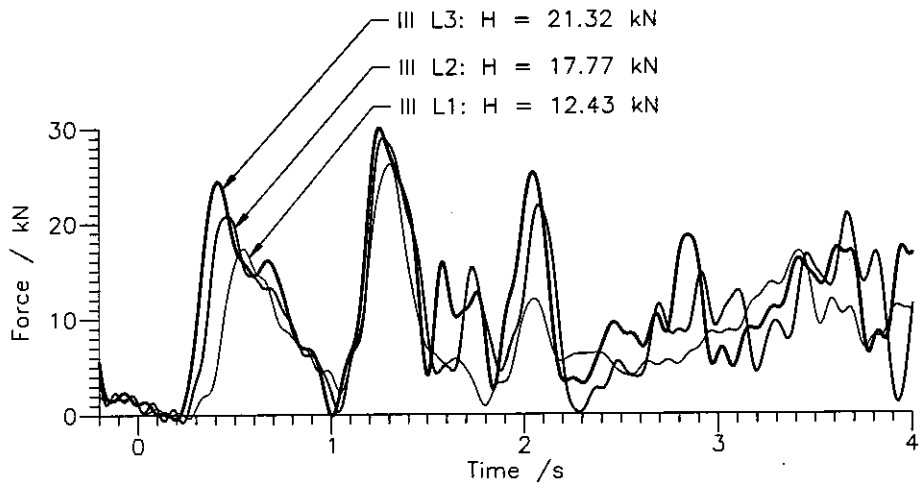
Insulator Tension at Tower T3  
Test III L2 vs Filtered ADINA Model

Figure 4-19



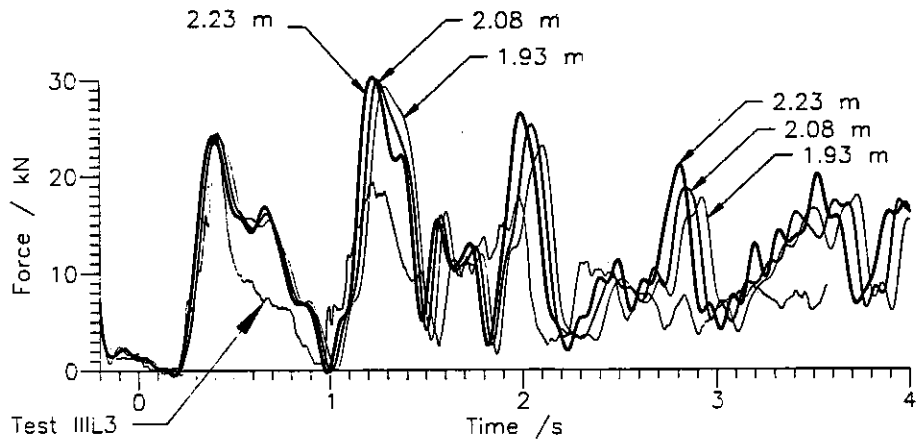
Insulator Tension at Tower T3  
Test III L3 vs Filtered ADINA Model

Figure 4-20



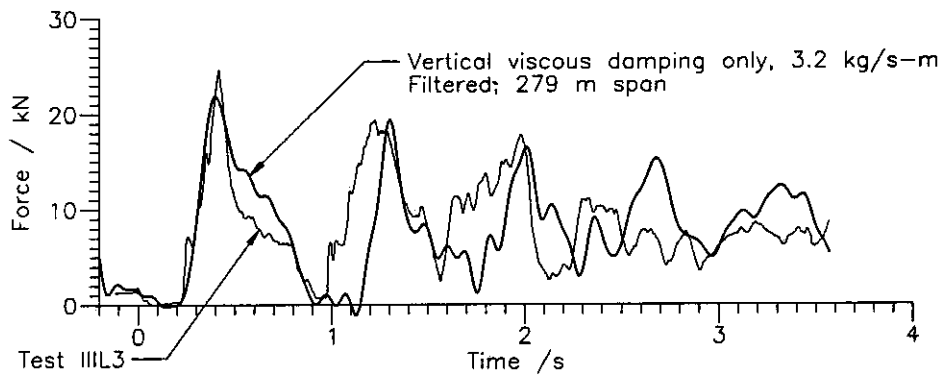
Insulator Tensions Tower T3  
ADINA Models of Tests III L1 to 3

Figure 4-21



Test III L3  
 Effect of Changes in Insulator Length

Figure 4-22



Insulator Tension at Tower T3  
Test vs ADINA Model with Vertical Damping

Figure 4-23

# **Appendix A**

## **Conductor Natural Frequencies and Mode Shapes**

### **A.1.1 Introduction**

Calculation of the natural frequencies of suspended cables is described in Irvine (1992). This method is based on a parabolic approximation to the catenary shape of a suspended wire. The following equations have been adapted from Irvine's description of the natural frequencies of inclined spans using the simplifications of Blevins (1979) and adopting the notation for describing the cable used by Ehrenburg (1935). Ehrenburg's is among the best presentations of methods for calculating the properties of a catenary cable, including formulas for calculating the position of the low point of sag in inclined spans, the effective tension, the stressed and unstressed lengths and other useful information.

The natural frequencies and mode shapes can be divided into three categories. The in-plane symmetric modes, the in-plane antisymmetric modes, and the out-of-plane modes. The in-plane modes occur in the plane defined by the sag of the cable. The first out of plane mode can be described as a pendulum mode in which the cable swings back and forth about its supports perpendicular to the plane of the cable at rest. The in-plane symmetric modes have an odd number of loops in a span while the in-plane antisymmetric modes have an even number of loops.

### A.1.2 In-Plane Antisymmetric Modes

Equation A-1 gives the natural frequencies of the in-plane anti-symmetric modes where  $a$  is the span,  $c$  is the chord length (the straight line distance between supports) in an inclined span,  $m$  is the unit mass per length of the cable and  $H$  is the horizontal component of the tension.

$$\omega_n = \frac{n\pi}{\sqrt{ac}} \sqrt{\frac{H}{m}} \quad n = 2, 4, 6, \dots \quad \text{Equation A-1}$$

### A.1.3 In-Plane Symmetric Modes

For both inclined and flat spans, equation A-2 gives the sag  $d$  based on the parabolic approximation to the catenary where  $w$  is the weight per unit length or  $mg$ . In the parabolic approximation, the unit weight of the cable is assumed to be uniform along the horizontal projection of the curve rather than along the arc length.

$$d = \frac{wa^2}{8H} \quad \text{Equation A-2}$$

Equation A-3 gives a parameter described by Blevins as the “virtual cable length.”

$$L_e = c \left[ 1 + 8 \left( \frac{d}{c} \right)^2 \right] \quad \text{Equation A-3}$$

The natural frequencies of the symmetric modes are calculated using the non-zero roots in  $\lambda$  of the transcendental equation shown in Equation A-4.

$$\tan \frac{\lambda\pi}{2} - \frac{\lambda\pi}{2} + \frac{4}{\alpha^2} \left( \frac{\lambda\pi}{2} \right)^3 = 0 \quad \text{Equation A-4}$$

Where  $\alpha$  is given by equation A-5,  $E$  is the modulus of elasticity and  $A$  is the cross-sectional area.

$$\alpha = \frac{8d}{c} \sqrt{\frac{EA_c}{HL_e}} \quad \text{Equation A-5}$$

The in-plane symmetric natural frequencies  $\omega_\lambda$  are given by equation A-6. Note the similarity to equation A-1 where  $n$  is replaced by  $\lambda$ .

$$\omega_\lambda = \frac{\lambda\pi}{\sqrt{ac}} \sqrt{\frac{H}{m}} \quad \text{Equation A-6}$$

A second method for calculating the in-plane symmetric natural frequencies was developed by Shears (1968). This method is also described in Peyrot et al. (1978) where it is used (in the fortran program CABLE5) to calculate the first symmetric inplane natural frequency of the first span of the copper conductor used in one of the EPRI Wisconsin tests. In this method, the symmetric natural frequencies are given by the solution of the eigenproblem in Equation A-7.

$$|K - \Omega I| = 0 \quad \text{Equation A-7}$$

$\Omega$  is the matrix of eigenvalues of  $K$ .  $K$  is given by Equation A-8 where  $\omega_n$  is given by equation A-1 with  $n = 1, 3, 5, \dots$  and  $\zeta$  is given by equation A-9.

$$K = \begin{bmatrix} \omega_1^2(1+\zeta) & \frac{\omega_1^2\zeta}{1^3 \cdot 3} & \frac{\omega_1^2\zeta}{1^3 \cdot 5} & \frac{\omega_1^2\zeta}{1^3 \cdot 7} & \frac{\omega_1^2\zeta}{1^3 \cdot 9} \\ \frac{\omega_1^2\zeta}{3^3 \cdot 1} & \omega_3^2 \left(1 + \frac{\zeta}{3^4}\right) & \frac{\omega_1^2\zeta}{3^3 \cdot 5} & \frac{\omega_1^2\zeta}{3^3 \cdot 7} & \frac{\omega_1^2\zeta}{3^3 \cdot 9} \\ \frac{\omega_1^2\zeta}{5^3 \cdot 1} & \frac{\omega_1^2\zeta}{5^3 \cdot 3} & \omega_5^2 \left(1 + \frac{\zeta}{5^4}\right) & \frac{\omega_1^2\zeta}{5^3 \cdot 7} & \frac{\omega_1^2\zeta}{5^3 \cdot 9} \\ \frac{\omega_1^2\zeta}{7^3 \cdot 1} & \frac{\omega_1^2\zeta}{7^3 \cdot 3} & \frac{\omega_1^2\zeta}{7^3 \cdot 5} & \omega_7^2 \left(1 + \frac{\zeta}{7^4}\right) & \frac{\omega_1^2\zeta}{7^3 \cdot 9} \\ \frac{\omega_1^2\zeta}{9^3 \cdot 1} & \frac{\omega_1^2\zeta}{9^3 \cdot 3} & \frac{\omega_1^2\zeta}{9^3 \cdot 5} & \frac{\omega_1^2\zeta}{9^3 \cdot 7} & \omega_9^2 \left(1 + \frac{\zeta}{9^4}\right) \end{bmatrix} \quad \text{Equation A-8}$$

$$\zeta = \frac{8AEw^2 a^5}{\pi^4 H^3 c^3} \quad \text{Equation A-9}$$

Then the in-plane symmetric natural frequencies are given by Equation A-10.

$$\overline{\omega}_n = \sqrt{\Omega_n} \quad \text{Equation A-10}$$

#### A.1.4 Out-of-Plane Modes

Equation A-11 gives the out-of-plane natural frequencies based on Irvine and Blevins.

$$\omega_n = \frac{n\pi}{\sqrt{ac}} \sqrt{\frac{H}{m}} \quad n = 1, 2, 3... \quad \text{Equation A-11}$$

It is interesting to compare the first natural frequency given by Equation A-11 with that of a physical pendulum (Young and Freedman 2000, Section 13-7, p409) in the form of a parabolic cable as given in Equation A-12.

$$\omega = \frac{\sqrt{10}}{a} \sqrt{\frac{H}{m}} \quad \text{Equation A-12}$$

For a level span where  $a = c$ , the ratio of the two natural frequencies is 0.993, very good agreement for the first pendulum mode derived in two different ways.

#### A.1.5 Natural Frequencies and Mode Shapes using ADINA

ADINA has the capability of calculating natural frequencies and mode shapes of a suspended cable modeled as prestressed truss elements. A mass proportional load is defined to provide starting vectors for the frequency analysis. Table A-1 compares the the natural frequencies calculated using ADINA with those calculated in accordance

with the theory described above (a visual basic computer program was written to solve equation A-4). Table 4-2 contains the conductor properties used for the IBIS conductor. Calculations were based on a 300 m span and horizontal component of tension of 14.4 kN.

**Table A-1**  
**Comparison of Frequencies (in Hz)**  
**Ibis: 300 m Span, H = 14.4 kN**

Mode	Blevins & Irvine	Shears & Peyrot	ADINA Frequency Analysis Elements in 300 m Span				
			300	120	60	30	15
Symmetric Modes							
1	0.4186	0.4192	0.4183	0.4184	0.4189	0.4179	0.4172
3	0.6814	0.6815	0.6798	0.6791	0.6787	0.6765	0.6794
5	1.1116	1.1115	1.1093	1.1078	1.1054	1.0959	1.0584
7	1.5532	1.5532	1.5501	1.5470	1.5405	1.5147	1.4140
Antisymmetric Modes							
2	0.4435	0.4435	0.4420	0.4416	0.4414	0.4408	0.4384
4	0.8870	0.8870	0.8851	0.8840	0.8828	0.8780	0.8588
6	1.3305	1.3305	1.3278	1.3256	1.3215	1.3052	1.2414
8	1.7741	1.7740	1.7703	1.7662	1.7565	1.7181	1.5697

Blevins, R. D. (1979). *Formulas for natural frequency and mode shape*, Van Nostrand Reinhold Co., New York.

Ehrenburg, D. O. (1935). "Transmission Line Catenary Calculations." *Transactions of the AIEE*, 54(7), 719-728.

Irvine, M. (1992). *Cable Structures*, Dover Publications, Inc., Mineola, New York.

Peyrot, A. H., Kluge, R. O., and Lee, J. W. (1978). "Longitudinal Loading Tests on a Transmission Line." EPRI EL-905, Electric Power Research Institute, Palo Alto, CA.

Shears, M. (1968). "Static and Dynamic Behaviour of Guyed Masts." Report No. 68-6, Structural Engineering Laboratory, University of California Berkeley, California, Berkeley, CA.

Young, H. D., and Freedman, R. A. (2000). *Sears and Zemansky's University Physics*, Addison-Wesley series in physics, Addison-Wesley, San Francisco.

## Appendix B

### ADINA Model Parameters for EPRI-Wisconsin Power & Light Tests

**Table B-1**  
**Test Catenary Constants**

Test	Horizontal Tension - H (kN)	Unit Weight - w (N/m)	H/w (m)
III L1	12.43	7.977	1558
III L2	17.77	7.977	2228
III L3	21.32	7.977	2673

**Table B-2**  
**Tower and Insulator Model Parameters**

Description	Value
Longitudinal Effective Mass	817 kg
Longitudinal Spring Constant	682 kN/m
Longitudinal Damping Constant	2360 kg/s
Longitudinal Damping Coefficient	5%
Longitudinal Frequency	4.60Hz
Torsional Effective Mass	4255 kg-m <sup>2</sup>
Torsional Spring Constant	8708 kN-m/rad
Torsional Damping Constant	19000 kg-m <sup>2</sup> /s
Torsional Damping Coefficient	5%
Torsional Frequency	7.2 Hz
Vertical Effective Mass	21100 kg-m <sup>2</sup>
Vertical Spring Constant	17620 kN-m/rad
Vertical Damping Constant	61000 kg-m <sup>2</sup> /s
Vertical Damping Coefficient	5%
Vertical Frequency	4.6 Hz
Insulator Length	2.08 m

**Table B-3  
Conductor Parameters**

<b>Description</b>	<b>Value</b>
Length of Span T3 to T4	297 m
Finite Element Length	2.5 m ±
Area	234 mm <sup>2</sup>
Density	3476 kg/m <sup>3</sup>
Modulus of Elasticity	74.2 GPa
Horizontal Tension	See Table B-1
Axial Viscous Damping Constant	37.58 kg/s
Axial Viscous Damping Coefficient	0.5%
Aerodynamic Drag Coefficient	1.25
Aerodynamic Damping Constant	0.381/m

**Table B-4  
Analysis Parameters**

<b>Description</b>	<b>Value</b>
Time Integration Method	Wilson-Theta (1.4)
Displacements	Large
Strains	Small
Equilibrium Iteration Method	BFGS
Calculation Time Step	0.1 ms
Time Interval for Saved Data	5.0 ms
Convergence Criteria	Energy & Displacement
Relative Energy Tolerance (ETOL)	0.10 E-06
Relative Displacement Tolerance (DTOL)	0.10 E-04
Line Convergence Tolerance (STOL)	0.10
Stiffness Matrix Update Frequency	Every Equilibrium Step